STRUCTURAL SCIENCE CRYSTAL ENGINEERING MATERIALS

ISSN 2052-5206

New superprotonic crystals with dynamically disordered hydrogen bonds: cation replacements as the alternative to temperature increase

Elena V. Selezneva,[a]* Irina P. Makarova,[a] Inna A. Malyshkina,[b] Nadezhda D. Gavrilova,[b] Vadim V. Grebenev,[a] Vitalii K. Novik[b] and Vladimir A. Komornikov[a]

[a]Shubnikov Institute of Crystallography of Federal Scientific Research Centre, 'Crystallography and Photonics', Russian Academy of Sciences, Leninsky prospect 59, Moscow, 119333, Russian Federation, and [b]Faculty of Physics, M.V. Lomonosov Moscow State University, Leninskye Gory 1, Moscow, 119991, Russian Federation. *Correspondence e-mail: msdmitricheva@yandex.ru

Received 7 June 2017
Accepted 7 September 2017

Edited by N. B. Bolotina, Russian Academy of Sciences, Russia

Keywords: single crystals; X-ray analysis; crystal structure; hydrogen bonds; superprotonic phase transitions; structural conditionality; conductivity.

CCDC reference: 1573140

Supporting information: this article has supporting information at journals.iucr.org/b

Investigations of new single crystals grown in the $K_3H(SO_4)_2$–$(NH_4)_3H(SO_4)_2$–H_2O system from solutions with different K:NH_4 concentration ratios have been carried out. Based on the X-ray diffraction data, the atomic structure of the crystals was determined at room temperature taking H atoms into account. It has been determined that $[K_{0.43}(NH_4)_{0.57}]_3H(SO_4)_2$ crystals are trigonal at ambient conditions such as the superprotonic phase of $(NH_4)_3H(SO_4)_2$ at high temperature. A distribution of the K and N atoms in the crystal was modelled on the basis of the refined occupancies of K/N positions. Studies of dielectric properties over the temperature range 223–353 K revealed high values of conductivity of the crystals comparable with the conductivity of known superprotonic compounds at high temperatures, and an anomaly corresponding to a transition to the phase with low conductivity upon cooling.

1. Introduction

The crystal family $M_mH_n(AO_4)_{(m+n)/2}\cdot yH_2O$ (M = K, Rb, Cs, NH_4, and AO_4 = S, Se, HPO_4, $HAsO_4$) is of special interest owing to its unique properties, especially high proton conductivity (see *e.g.* Ramasastry & Ramaiah, 1981; Baranov *et al.*, 1982, 1989; Pawlowski *et al.*, 1990), which are conditioned by the hydrogen-bond network rearrangement (see *e.g.* Mkarova *et al.*, 1988; Łukaszewicz *et al.*, 1993; Melzer, 1996; Chen *et al.*, 2000; Matsuo *et al.*, 2002; Baranov, 2003; Lim & Ichikawa, 2006; Ivanov-Schitz & Murin, 2010; Pavlenko *et al.*, 2011; Makarova, 2015). Because of the high proton conductivity, the value of which is close to the conductivity of the melts of these salts (10^{-3}–10^{-1} Ω^{-1} cm^{-1}), these crystals are promising materials for various electrochemical devices, including proton exchange membranes in fuel cells (see *e.g.* Norby, 2001; Fitzergerald, 2001; Otomo, 2003; Haile *et al.*, 2007).

A systematic study of the salt system of $K_3H(SO_4)_2$–$(NH_4)_3H(SO_4)_2$–H_2O solid solutions and crystal growth was performed for the first time at the Shubnikov Institute of Crystallography of the Russian Academy of Sciences (IC RAS) (see *e.g.* Dmitricheva *et al.*, 2014*a*,*b*; Dmitricheva *et al.*, 2014, 2015; Selezneva *et al.*, 2018). It was found that solutions of $K_3H(SO_4)_2$ and $(NH_4)_3H(SO_4)_2$ with different K:NH_4 ratios

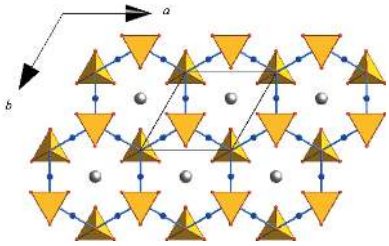

crystallize in different structure types. Using $K_3H(SO_4)_2$ and $(NH_4)_3H(SO_4)_2$ solutions with a K:NH_4 ratio close to 1:1, one can grow single crystals with a structure type different from that of the initial compounds: the chemical formula of the grown single crystals is $[K_{1-x}(NH_4)_x]_9H_7(SO_4)_8{\cdot}H_2O$ (see *e.g.* Dmitricheva *et al.*, 2014*a*,*b*). A comparison of the data on the $K_9H_7(SO_4)_8{\cdot}H_2O$ (Makarova *et al.*, 2014) and $[K_{1-x}(NH_4)_x]_9H_7(SO_4)_8{\cdot}H_2O$ crystals (Dmitricheva *et al.*, 2014*b*) showed that the replacement of potassium with ammonium, even $\simeq$4%, reduced the temperature of structural phase transition by 8 K. At the same time, the formation of additional hydrogen bonds between NH_4 and SO_4 groups, which block the conductivity channels for K ions, leads to a decrease in conductivity by four orders of magnitude, which indicates simultaneously the contribution of K ions to the conductivity of the $(K,NH_4)_9H_7(SO_4)_8{\cdot}H_2O$ compound.

$K_3H(SO_4)_2$ and $(NH_4)_3H(SO_4)_2$ solutions with a ratio of 9:1 were used to grow crystals of the same structure type as $K_3H(SO_4)_2$; the single crystals were described by the chemical formula $[K_{1-x}(NH_4)_x]_3H(SO_4)_2$ (Dmitricheva *et al.*, 2014; Selezneva *et al.*, 2018). Based on the refined structural model, it has been concluded that the $[K_{1-x}(NH_4)_x]_3H(SO_4)_2$ samples contain no less than 3% ammonium. This amount of ammonium is found to be sufficient to change significantly the kinetics of structural phase transitions in comparison with $K_3H(SO_4)_2$ crystals; this is related to the formation of additional hydrogen bonds and the change in the anisotropy of the coordination environment of both cations and SO_4 tetrahedra.

This paper reports the results of research on single crystals grown in the $K_3H(SO_4)_2$–$(NH_4)_3H(SO_4)_2$–H_2O system from solutions with a K:NH_4 concentration ratio of $\sim$3:7.

2. Experimental details

Single crystals of $(K,NH_4)_3H(SO_4)_2$ were grown by controlled reduction of solubility. Growth solutions were prepared using K_2SO_4, $(NH_4)_2SO_4$ and H_2SO_4 reagents. The crystals were grown by combining synthesized stoichiometric solutions. Crystallization was carried out over the temperature range of 303–313 K. Solutions with a K:NH_4 concentration ratio of 3:7 yielded large single crystals with high optical activity suitable for study. Pseudo-hexagonal thin plates were grown with the predominant face (001) (Fig. 1).

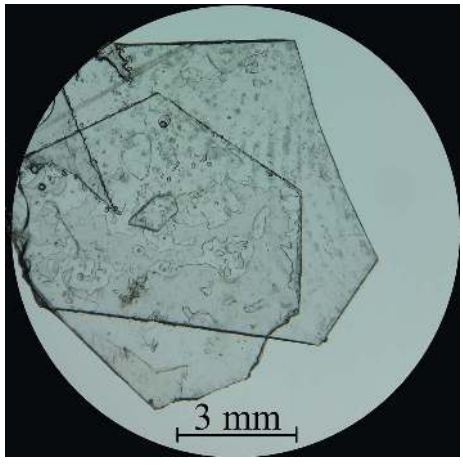

Figure 1
Single crystals of $[K_{0.43}(NH_4)_{0.57}]_3H(SO_4)_2$.

Table 1
Experimental details.

Crystal data	
Chemical formula	$[K_{0.43}(NH_4)_{0.57}]_3H(SO_4)_2$
M_r	274.41
Crystal system, space group	Trigonal, $R\overline{3}$
Temperature (K)	293
a, c (Å)	5.7768 (3), 22.0983 (12)
V (Å^3)	638.65 (8)
D_x (g cm^{-3})	2.023
Z	3
Radiation type	Mo $K\alpha$
μ (mm^{-1})	1.276
Crystal size (mm)	0.20 × 0.17 × 0.15
Data collection	
Diffractometer	Xcalibur, Sapphire3 with high theta cut
Absorption correction	Multi-scan using *CrysAlis PRO*; empirical absorption correction using spherical harmonics, implemented in *SCALE3 ABSPACK*
Scan mode	ω
T_{min}, T_{max}	0.935, 1
θ_{max} (°)	32.72
No. of measured, independent and observed [$I > 3\sigma(I)$] reflections	4750, 533, 490
R_{int}	0.018
(sin $\theta/\lambda)_{max}$ (Å^{-1})	0.767
Refinement	
$R[F^2 > 2\sigma(F^2)]$, $wR(F^2)$, S	0.027, 0.038, 2.46
Refinement based on F with a weighting scheme	w = 1/$\sigma^2(F)$
No. of reflections	490
No. of parameters	60
Extinction coefficient (isotropic, type 1)	0.09 (4)
H-atom treatment	H-atom parameters constrained
$\Delta\rho_{max}$, $\Delta\rho_{min}$ (e Å^{-3})	0.18, −0.30

CrysAlis PRO, *SCALE3 ABSPACK* (Oxford Diffraction, 2011), *JANA*2006 (Petříček *et al.*, 2014.

Studies of the chemical composition of the single crystals grown were performed with a Quanta 3D scanning electron microscope (FEI, USA) equipped with an EDXS attachment for X-ray energy-dispersive microanalysis (EDAX Inc., Mahwah, NJ, USA) using an accelerating voltage of 15 kV under high vacuum (6.95 Pa). Spectra were obtained from fresh cleavages of single crystals. Elemental compositions were calculated using the *EDAX* program (Edax Inc., Mahwah, NJ, USA) with due regard for the atomic number, absorption and fluorescence.

The X-ray diffraction studies of single crystals were carried out on an Xcalibur S diffractometer (Oxford Diffraction) with a CCD area detector. The experimental data were processed using *CrysAlis PRO* (Oxford Diffraction, 2011). The diffraction intensities were converted to structure-factor amplitudes, taking into account the kinematic and polarization factors. Structure refinement was carried out using *JANA2006* (Petříček *et al.*, 2014). The final values of structural parameters

were refined by the full-matrix least-squares method. Corrections for secondary extinction were made following the Becker–Coppens formalism (Becker & Coppens, 1974). Table 1 summarizes the main crystallographic characteristics, experimental diffraction data and the results of the refinements of the $(K,NH_4)_3H(SO_4)_2$ structure at room temperature.

The dielectric spectroscopy studies were carried out in an isothermal regime in the temperature interval 223–353 K and the frequency range 10^{-1}–10^7 Hz using a broadband dielectric spectrometer (Novocontrol Concept 40). The sample used here was 3 mm × 4 mm × 0.44 mm and had a plate-like form with dominant (001) faces. Silver paste served as the electrodes.

3. Results and discussion

3.1. Structural analysis

Our study shows that the crystals grown belong to the same structure type as the high-temperature phase of $(NH_4)_3H(SO_4)_2$ (Fukami *et al.*, 1996). The X-ray diffraction pattern for the $(K,NH_4)_3H(SO_4)_2$ sample in the plane *hk*0 of reciprocal space is shown in Fig. 2, which confirms the trigonal symmetry. The analysis of the systematic absences and symmetry-equivalent reflections indicates two possible space groups $R\bar{3}m$ and $R\bar{3}$ for the room-temperature structure. The structure refinement in the more symmetrical model (space group $R\bar{3}m$) meant that it was not possible to reduce discrepancy indices below R/wR = 0.17/0.22; any attempts to take into account the occupancy q of atomic sites led to the q values having no physical meaning. In view of this, further calculations were performed using the space group $R\bar{3}$.

To refine the crystal structure of the $(K,NH_4)_3H(SO_4)_2$ sample, the coordinates of the basic non-H atoms from Dmitricheva *et al.* (2015) were used as the initial data. Using the refined structural parameters, the difference electron-density maps from the complete set of reflections were calculated (Fig. 3). The electron-density distribution demonstrates a residual positive peak between O1 and O1′ positions related by the O1—H1···O1′ hydrogen bond with the H1 atom not included in the structural model (Fig. 3*a*). The refinement of the structure model including the H1 atom led to the discrepancy indices R/wR = 0.15/0.20 (disregarding the replacement of K atoms with NH_4). The difference electron-density maps were calculated at this stage (Fig. 3*b*) with $\Delta\rho_{min}/\Delta\rho_{max}$ = −2.32/2.49 e Å^{-3}. The inclusion of the H atom in the model led to the map clearance between O1 and O1′. At the same time, disorder of the O atoms was observed as shown by the residual values near their positions.

Occupancies of K/N positions ($q_K + q_N$ = 1.0) were refined in order to determine the potassium and nitrogen contents (for K1/N1 and K2/N2 positions independently, the thermal displacement parameters of K and N were assumed to be equal). To provide the most efficient estimation, the dependence of R factor on the q value was calculated ('stepwise scanning'). The occupancies of K1/N1 and K2/N2 sites were obtained as follows: q_{K1} = 0.80 (2) and q_{N1} = 0.20 (2); q_{K2} = 0.25 (1) and q_{N2} = 0.75 (1) corresponding to ≃57% [or 5.0 (2) atoms] of the nitrogen content per unit cell. With allowance for the replacement of K atoms with N in the structural model, R factors decreased to R/wR = 0.052/0.085 ($\Delta\rho_{min}/\Delta\rho_{max}$ = −0.57/0.97 e Å^{-3}).

Consideration of anharmonicity showed a significant deviation of atomic displacement parameters from the harmonic approximation only for O atoms, with the values of other anharmonic parameters being effectively harmonic within the relevant standard uncertainties. For two O atoms, in correspondence with the site symmetry, there are 102 refined anharmonic parameters, to the sixth order inclusively. Among

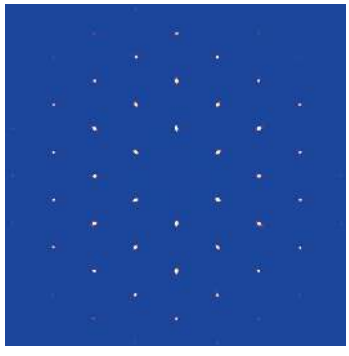

Figure 2
X-ray diffraction pattern for the $[K_{0.43}(NH_4)_{0.57}]_3H(SO_4)_2$ sample at the *hk*0 plane of reciprocal space.

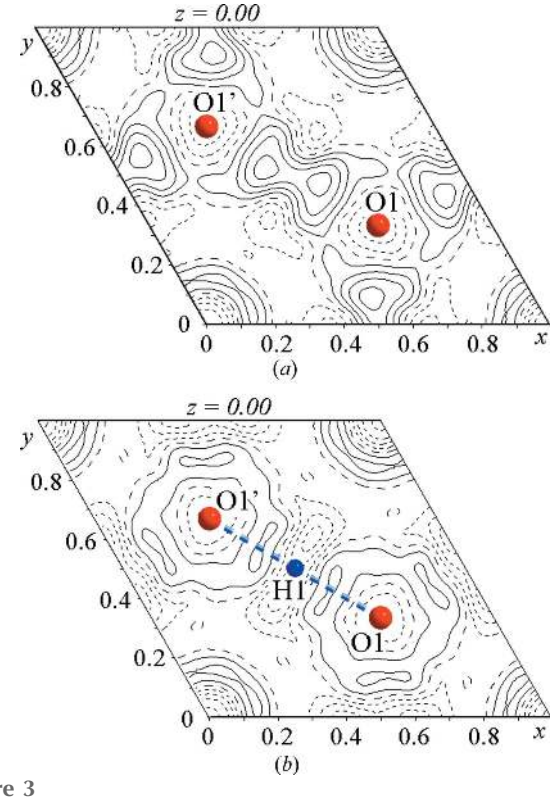

Figure 3
Difference electron-density maps: the H1 atom is disregarded (*a*); the H1 atom is taken into account (*b*). Positive (solid lines) and negative (dotted lines) contour intervals are 0.03 e Å^{-3}. O1 atoms are shown, which are located near this cross section.

Table 2
Wyckoff positions and occupancies (q), atomic coordinates (x/a, y/b, z/c), and effective isotropic atomic displacement parameters (U) for the basic atoms in the crystal structure of $[K_{0.43}(NH_4)_{0.57}]_3H(SO_4)_2$ at 293 K.

H atoms were refined with isotropic thermal parameters. O atoms were refined in the anharmonic approximation (to the sixth order inclusively).

Atoms	Wyckoff position	q	x/a	y/b	z/c	U (Å^2)
K1/N1	3*a*	0.80 (2)/0.20 (2)	0	0	0	0.039 (1)
K2/N2	6*c*	0.25 (2)/0.75 (2)	0	0	0.20082 (9)	0.046 (1)
S	6*c*	1	0	0	0.40761 (2)	0.036 (1)
O1†	6*c*	1	0	0	0.3398 (1)	0.087 (1)
O2‡	18*f*	1	0.1371 (2)	−0.1367 (3)	0.57250 (6)	0.054 (1)
H1	9*e*	0.33	0.5	0	0	0.08 (1)
H2	18*f*	0.75	0.07 (3)	0.17 (3)	0.21 (3)	0.09 (7)
H3	6*c*	0.75	0	0	0.15 (2)	0.09 (7)
H4	18*f*	0.1	0.07 (3)	0.15 (3)	0.02 (1)	0.06 (5)
H5	6*c*	0.1	0	0	−0.06 (2)	0.07 (8)

† O1: $C^{111} = -0.08$ (2), $C^{112} = -0.04$ (2), $C^{113} = -0.002$ (1), $D^{1111} = -0.13$ (2), $E^{11111} = 0.41$ (5), $E^{11112} = 0.20$ (3), $F^{111122} = -0.07$ (3), $F^{111133} = 0.0010$ (4). ‡ O2: $C^{133} = -0.0006$ (1), $C^{233} = 0.0007$ (1), $C^{333} = 0.00059$ (5), $D^{1112} = 0.009$ (2), $D^{1123} = -0.0015$ (4), $D^{1133} = 0.0004$ (1), $D^{1222} = 0.009$ (3), $D^{1233} = 0.0004$ (1), $D^{2222} = 0.005$ (5), $D^{2233} = 0.0004$ (2), $E^{11122} = 0.0019$ (5), $E^{12222} = -0.004$ (2), $E^{22222} = -0.013$ (5), $F^{111111} = -0.008$ (5), $F^{111122} = -0.002$ (1), $F^{111123} = -0.0006$ (3), $F^{112222} = -0.003$ (1).

them, 25 parameters were chosen which exceeded standard deviations (Table 2).

The consideration of anharmonic parameters led to a decrease in the residual peaks in electron-density maps near O1 and O2 atoms and reduced R factors to $R/wR = 0.028/0.041$ (the $\Delta\rho_{min}/\Delta\rho_{max}$ ratio is $-0.44/0.28$ e Å^{-3}). The partial substitution of tetrahedral ammonium groups by K atoms allowed the NH_4 tetrahedrons to realize their inner axis of symmetry of the third order, building the corresponding coordination sphere, which led to the formation of the trigonal symmetry in the entire crystal. Observed deviations from harmonic approximation in displacement parameters of O atoms indicate dynamical disordering of O positions due to the increase of symmetry.

The calculated electron-density distribution demonstrates residual positive peaks near N1 (Figs. 4*a*, 4*b*) and N2 (Figs. 5*a*, 5*b*) positions corresponding to the H atoms of ammonium groups, which have been lacking in the structural model till now. The positions of the H2, H3 and H4 atoms were determined from the difference electron-density maps. The coordinates of the H5 atom were calculated from the reasonable geometry of tetrahedral NH_4 groups. After H atoms of

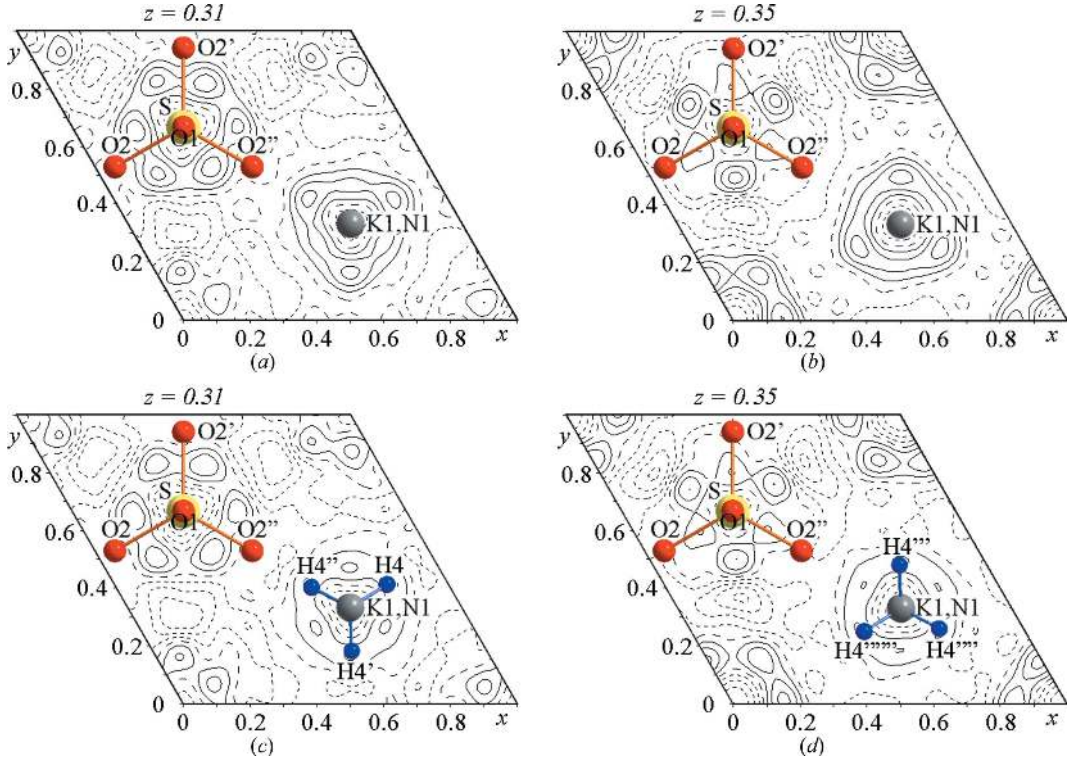

Figure 4
Difference electron-density maps: the H4 atoms are disregarded (*a*), (*b*); the H4 atoms are taken into account (*c*), (*d*). Positive (solid lines) and negative (dotted lines) contour intervals are 0.03 e Å^{-3}. S, O1, O2, K1/N1 positions are shown, which are located near this cross section.

Table 3
Main interatomic distances in the crystal of $[K_{0.43}(NH_4)_{0.57}]_3H(SO_4)_2$.

Bond	Distance (Å)
K1—O2 ×6	2.863 (2)
K1—O1 ×6	3.338 (1)
K2—O2 ×3	3.024 (1)
K2—O2′ ×3	3.026 (2)
K2—O2″ ×3	3.069 (2)
K2—O1	3.072 (3)
S—O2 ×3	1.438 (2)
S—O1	1.498 (3)

ammonium groups were taken into account, R factors decreased to R/wR = 0.027/0.038 ($\Delta\rho_{min}/\Delta\rho_{max}$ = −0.30/0.18 e Å^{-3}). The chemical formula of the crystal was finally determined as $[K_{0.43}(NH_4)_{0.57}]_3H(SO_4)_2$. The refined positional and atomic displacement parameters for the basic atoms of the crystal structure are given in Table 2. The main interatomic distances for the refined structural model are listed in Table 3.

Fig. 6(*a*) shows a model of the atomic structure of the crystal under study. The independent part of the unit cell contains two K atoms at (0, 0, 0) and (0, 0, z) positions, one S atom at a (0,0, z) position, and two O atoms: O1 (0, 0, z) and O2 (x, y, z). The SO_4 tetrahedron contains one elongated S—O1 bond with a length of 1.498 (3) Å and three equal S—O2 bonds with a length of 1.439 (1) Å (Fig. 7). The vertices of the SO_4 tetrahedra are connected by O1—H1···O1′ hydrogen bonds 3.348 (1) Å long. This value corresponds to the distance between central positions O1 on the threefold axis whereas the atoms themselves undergo thermal vibrations, which are essentially anharmonic. The O1 atom, which is involved in hydrogen bonds, forms the longest S—O bond and occupies a dynamically disordered position which means that O1 changes its position each time forming O1—H···O1′ bonds. O1 changes its position, which leads to the formation of new temporary O1—H···O1′ bonds.

Thus, the main structural motif is a double layer of SO_4 tetrahedra whose vertices are linked by hydrogen bonds (Fig. 6*b*). The hydrogen-bonded system is a two-dimensional network of hydrogen bonds, which is characterized by a dynamic disordering of both the positions of H atoms and the orientation of hydrogen bonds, similar to the high-temperature phase of other members of the $M_3H(AO_4)_2$ family, for example, $Rb_3H(SeO_4)_2$ (Mkarova *et al.*, 1988) or $K_3H(SO_4)_2$ (Makarova *et al.*, 2010).

The refinement of the structure reveals that the $[K_{0.43}(NH_4)_{0.57}]_3H(SO_4)_2$ crystal contains about 57% ammonium, which leads to the formation of an additional hydrogen subsystem. These data are in good agreement with structural parameters obtained by using synchrotron radiation at the SNBL BM01A experimental station of the European Synchrotron Radiation Facility, Grenoble (data to be published).

Thus, the ratios of K/N are 5/1 in the K1/N1 position and 1/3 in the K2/N2 position. Such values can be described by 6 × 6 cells with 144 atoms of K and 180 atoms of N. The corre-

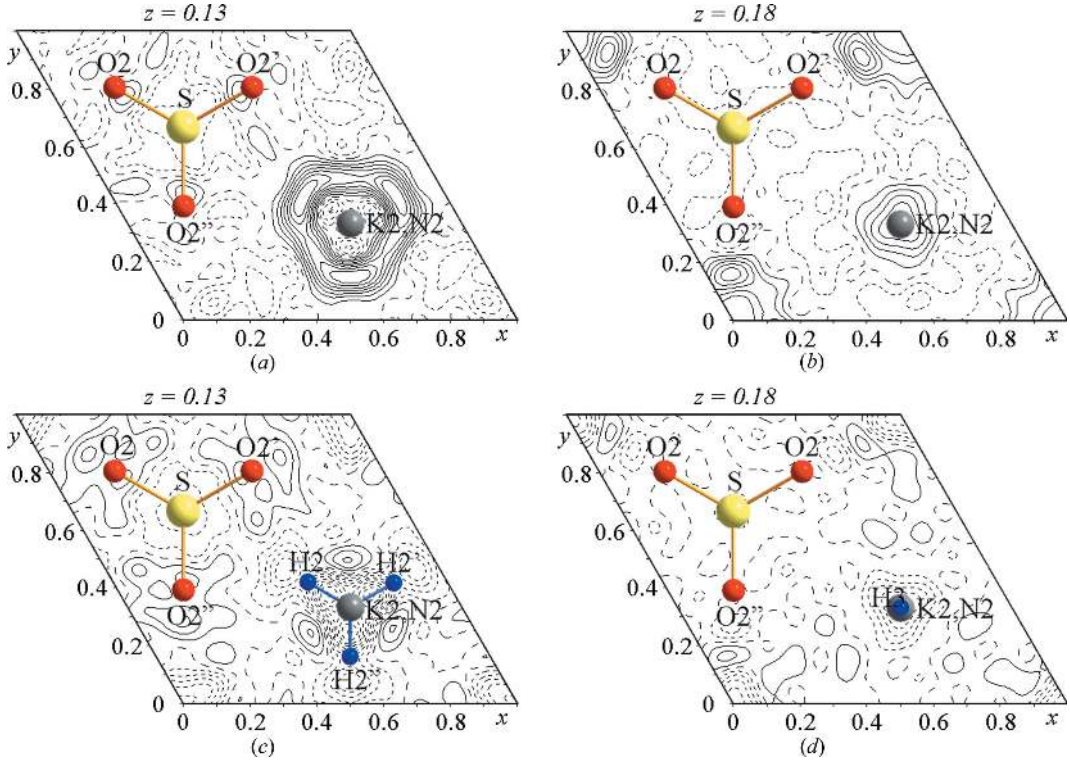

Figure 5
Difference electron-density maps: H2 (*a*) and H3 (*b*) atoms are disregarded; the H2 (*c*) and H3 (*d*) atoms are taken into account. Positive (solid lines) and negative (dotted lines) contour intervals are 0.03 e Å^{-3}. S, O2, K2/N2 positions are shown, which are located near this cross section.

sponding model of the distribution of the K and N atoms in the crystal is shown in Figs. 8(*a*) and 8(*b*). Most of the ammonium groups replace potassium in the K2/N2 position located between the layers of SO_4 tetrahedra. This leads to the binding of these layers by additional hydrogen bonds, and at the same time the symmetry of the coordination environment of the cations changes and the axis of symmetry of the third-order forms (Fig. 8*c*). The fact that the $[K_{0.43}(NH_4)_{0.57}]_3H(SO_4)_2$ crystals have lower symmetry than the $(NH_4)_3H(SO_4)_2$ and $K_3H(SO_4)_2$ crystals can be explained by the replacement of potassium with ammonium. Replacements in the cation sublattice lead to a decrease in symmetry.

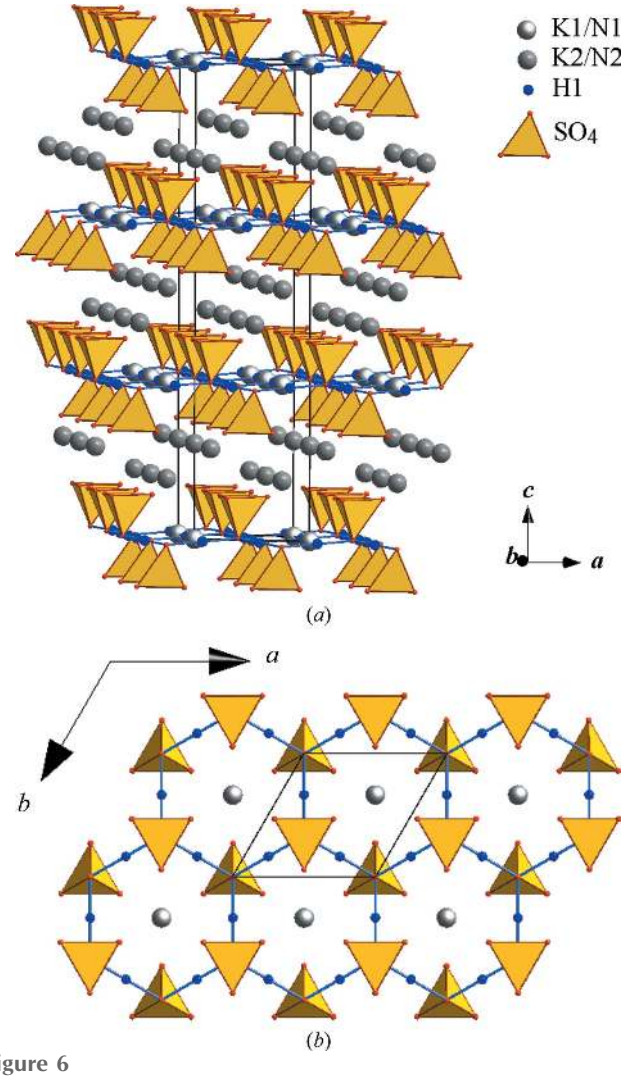

Figure 6
Atomic structure of the $[K_{0.43}(NH_4)_{0.57}]_3H(SO_4)_2$ crystals: (*a*) the K1/N1 and K2/N2 positions, SO_4 tetrahedron and hydrogen bonds are shown; (*b*) the system of hydrogen bonds.

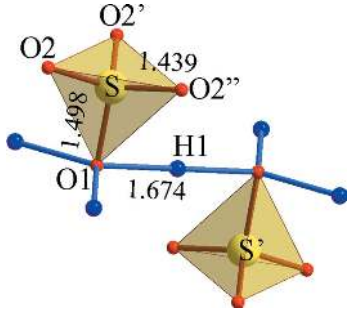

Figure 7
Main interatomic distances are shown in $(SO_4)\cdots H\cdots(SO_4)$ dimer.

3.2. Chemical analysis

According to the results of chemical analysis, the use of $K_3H(SO_4)_2$ and $(NH_4)_3H(SO_4)_2$ solutions with a ratio of 3:7 leads to the growth of crystals containing K^+ 9.82 mol% and

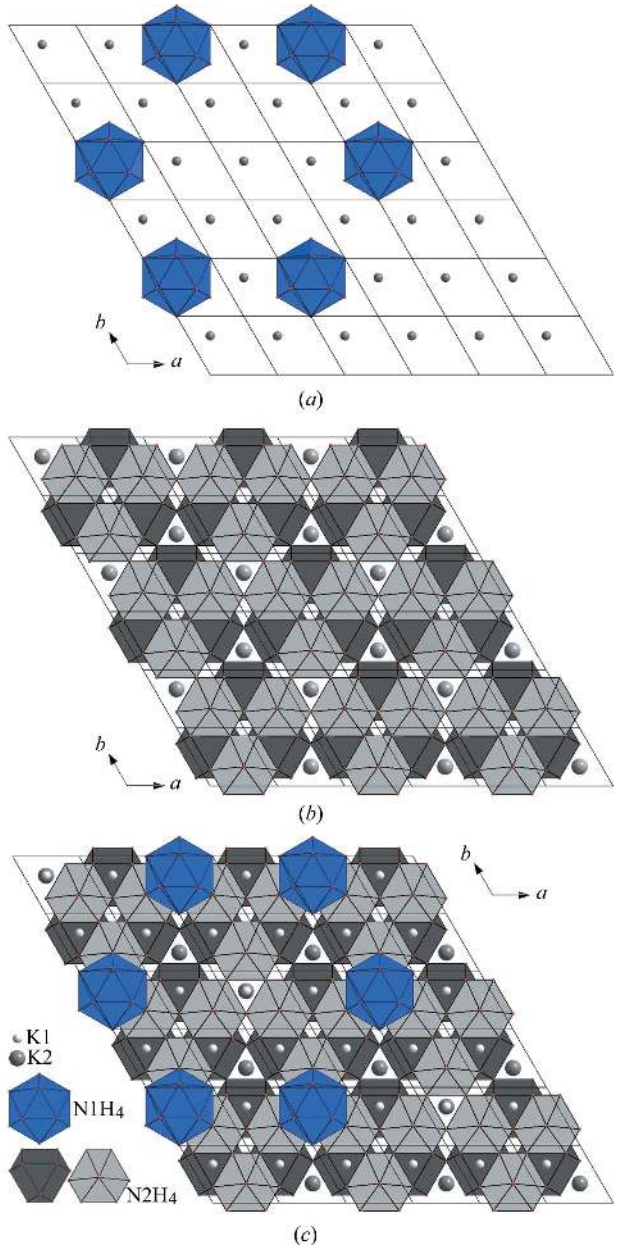

Figure 8
Systematic arrangement of K and N atoms in the $[K_{0.43}(NH_4)_{0.57}]_3H(SO_4)_2$ crystals: the layer with K1/N1 positions (*a*); the double layer with K2/N2 positions (*b*); the layers with K1/N1 and K2/N2 positions together (*c*). SO_4 tetrahedra and hydrogen bonds with H1 are omitted.

N^+ 13.61 mol% (K:N $\simeq$ 0.42:0.58). These results are in good agreement with occupancies of K/NH_4 positions refined from structural analysis.

3.3. Dielectric properties

The measurements were carried out along the *c* axis. Measurements along this direction allow us to estimate the binding layers of SO_4 tetrahedra due to additional hydrogen bonds between NH_4 and SO_4 groups. Conductivity in isostructural crystals of $K_3H(SO_4)_2$ and $(NH_4)_3H(SO_4)_2$ is not isotropic (the highest values are observed perpendicular to the *c* axis, because the system of hydrogen bonds is parallel to the *ab* plane). However, the small thickness of the samples under study does not allow measurements in the plane.

Fig. 9 represents the frequency dependence of the real ε' and imaginary ε'' parts of the dielectric permittivity, the AC conductivity σ_{AC} and dielectric loss tangent $\tan\delta$ for various temperatures. On the $\varepsilon'(f)$ plots (Fig. 9*a*) one observes at high frequencies a limiting constant value ε'_∞, which is related to the fast polarization processes occurring in the material. This value increases with temperature from $\varepsilon'_\infty = 18$ at 223 K to 28 at 353 K. With decreasing frequency $\varepsilon'(f)$ increases and shows a 'step' (which is more pronounced at low temperatures). In the same frequency range a 'structure' (a 'shoulder' on the high-frequency side of the peak) is observed on $\varepsilon''(f)$ spectra (Fig. 9*b*), which is a manifestation of a dielectric polarization process. This dispersion region shifts to higher frequencies with increasing temperature which indicates a thermally activated process.

At even lower frequencies $\varepsilon'(f)$ and $\varepsilon''(f)$ show a rapid increase and demonstrate giant values ($\sim 10^3$), which obviously do not correspond to the bulk properties of the material. In this frequency range random diffusion of the ionic charge carriers *via* activated hopping gives rise to a frequency-independent conductivity characterizing the conductivity σ_{DC} (Fig. 9*c*), whose values increase with increasing temperature from $10^{-9}\ \Omega^{-1}\,cm^{-1}$ at 223 K to $\sim 3 \times 10^{-4}\ \Omega^{-1}\,cm^{-1}$ at 353 K. For comparison, the $(NH_4)_3H(SO_4)_2$ crystals have the value $\sigma_{DC} \sim 10^{-4}\ \Omega^{-1}\,cm^{-1}$ at 425 K (Schwalowsky *et al.*, 1998). Simultaneously the plateau region shifts to higher

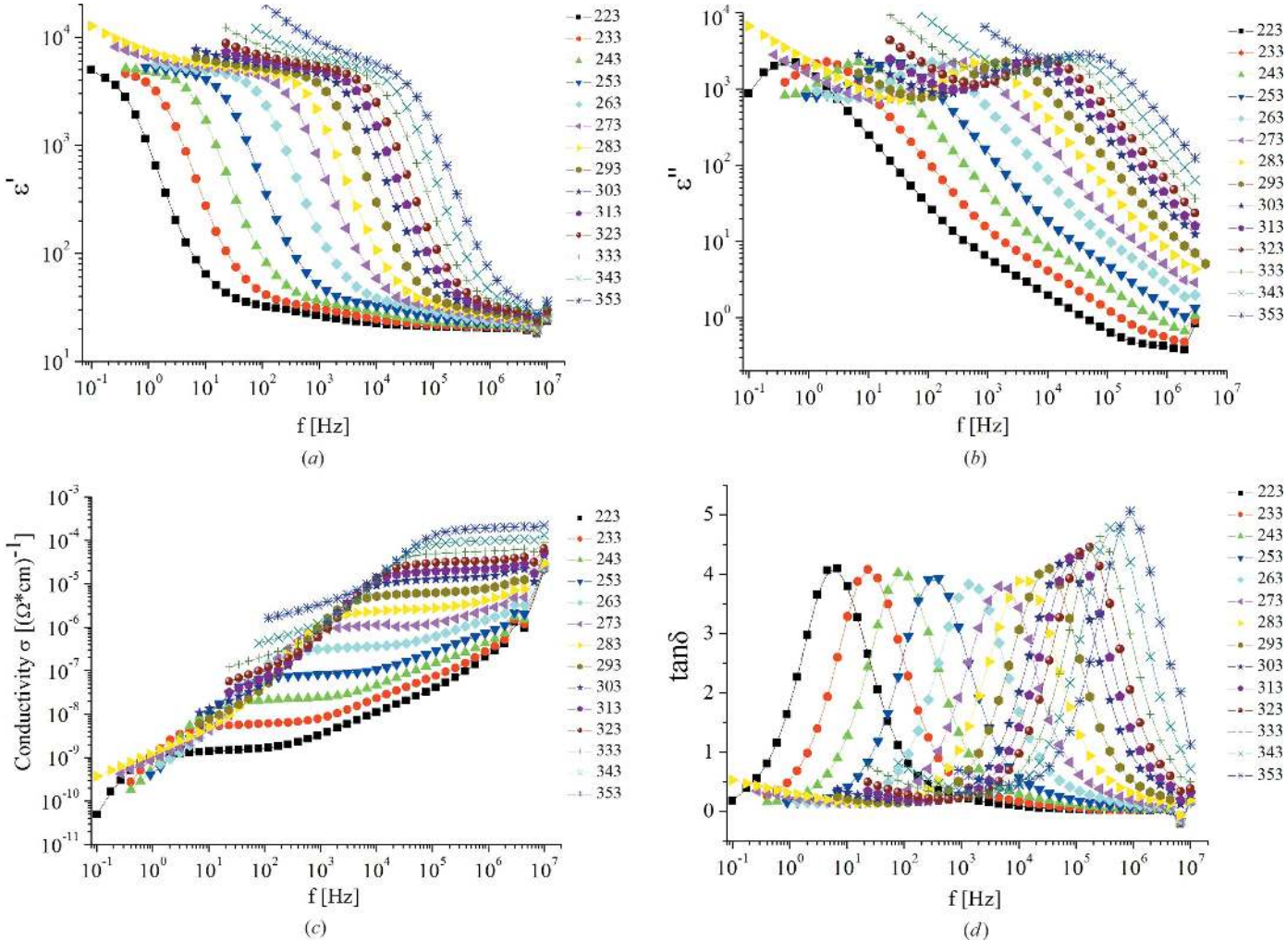

Figure 9
Frequency dependencies of the real ε' (*a*) and imaginary ε'' (*b*) parts of complex dielectric permittivity, AC conductivity (*c*) and $\tan\delta$ (*d*) at different temperatures indicated on the plot.

frequencies indicating that the conductivity is a thermally activated process. Thus, the high values of $\varepsilon'(f)$ and $\varepsilon''(f)$ are due to the charge carrier motion within the sample. Moreover, σ in Fig. 9(*c*) decreases with decreasing frequency at very low frequencies and high temperatures, and this drop correlates with a peak in $\varepsilon''(f)$ and a 'saturation' of $\varepsilon'(f)$ at very low frequencies. Such a behaviour at very low frequencies and high temperatures is typical of a high ionic conductor and can be ascribed to the processes of electrode polarization (MacDonald, 1987), which result from the presence of blocking electrodes, where a space charge 'builds up' resulting in a large bulk polarization.

The temperature dependence of the DC conductivity σ_{DC} is presented in Fig. 10 in Arrhenius coordinates. It is clearly seen that there is a change in the slope of the curve at $T \sim 283$ K. Below and above this temperature the data can be described well by the Arrhenius equation

$$\sigma_{DC} = \frac{A}{T}\exp\left(\frac{-U}{kT}\right), \quad (1)$$

where U is the activation energy, k is the Boltzmann constant. Below 283 K U = 0.72 eV and above this temperature U = 0.52 eV. The difference in the activation energies means that at 283 K there is a possible structural transition that changes the energy landscape for the drifting ions. Additional evidence for the existence of a structural transition can be seen in the frequency dependencies of the dielectric loss tangent, $\tan\delta = \varepsilon''/\varepsilon'$, given in Fig. 9(*d*) for various temperatures. The relatively large values of $\tan\delta$ confirm the important contribution of the DC conductivity to the dielectric permittivity in this material. The $\tan\delta(f)$ plots exhibit well defined peaks, which shift to higher frequencies with increasing temperature. The peaks are observed in the frequency region of the DC conductivity (Fig. 9*c*) indicating that they are related to the conductivity relaxation. It is interesting to follow the dependence of the magnitude of the $\tan\delta$ peak on temperature: below 273 K it decreases with increasing temperature, and it increases above 283 K. This temperature interval agrees fairly well with the temperature at which the conductivity activation energy changes (Fig. 10). This fact can serve as another indication of structural changes in the material in this temperature interval affecting conductive properties.

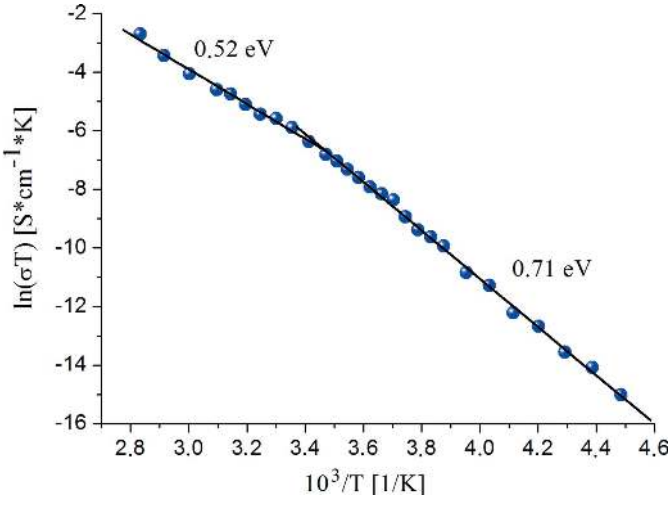

Figure 10
Arrhenius plot of the conductivity for the $[K_{0.43}(NH_4)_{0.57}]_3H(SO_4)_2$ crystal.

The values obtained for the activation energies U = 0.72 eV and U = 0.52 eV for the phases of $[K_{0.43}(NH_4)_{0.57}]_3H(SO_4)_2$ crystals correspond to the values U = 0.76 eV and U = 0.47 eV for the low- and high-temperature phases, respectively, of $(NH_4)_3H(SeO_4)_2$ crystals (Lindner *et al.*, 2014). The transition from the high-temperature $R\bar{3}$ phase to the high-temperature $R\bar{3}m$ phase in $(NH_4)_3H(SeO_4)_2$ is accompanied by a decrease in the activation energy to U = 0.33 eV.

4. Conclusion

Based on a systematic study of the salt system of $K_3H(SO_4)_2$–$(NH_4)_3H(SO_4)_2$–H_2O solid solutions, one may conclude that the use of $K_3H(SO_4)_2$ and $(NH_4)_3H(SO_4)_2$ solutions with different K/N ratios leads to the growth of single crystals of distinct structure types with varied physical properties.

The use of $K_3H(SO_4)_2$ and $(NH_4)_3H(SO_4)_2$ solutions with a K/N ratio of $\simeq$3:7 leads to the growth of crystals of the same structure type as the high-temperature superprotonic phase of $(NH_4)_3H(SO_4)_2$ (space group $R\bar{3}$).

In contrast to the known members of the family $M_3H(AO_4)_2$ (M = K, Rb, Cs, NH_4; AO_4 = SO_4, SeO_4, HPO_4, $HAsO_4$) that have a superprotonic phase transition with an increase in symmetry from monoclinic to trigonal at heating, the crystals of $[K_{0.43}(NH_4)_{0.57}]_3H(SO_4)_2$ have a superprotonic trigonal phase under ambient conditions. Trigonal symmetry is conditioned by the K/N occupation ratio and the corresponding coordination of NH_4 groups. The appearance of the threefold axis leads to disordering of the O atoms involved in hydrogen bonds and as a result to the formation of a dynamically disordered network of hydrogen bonds.

The dielectric properties of the crystal are mainly influenced by its high DC conductivity, which increases from 10^{-9} Ω^{-1} cm^{-1} at 223 K to $\sim 3 \times 10^{-4}$ Ω^{-1} cm^{-1} at 353 K. It is found that the conductivity is thermally activated below and above $T \sim 283$ K with corresponding activation energies of 0.72 and 0.52 eV. This critical temperature probably corresponds to the structural transition at which the symmetry of the $[K_{0.43}(NH_4)_{0.57}]_3H(SO_4)_2$ crystals changes.

Acknowledgements

We are grateful to V. V. Dolbinina (FSRC 'Crystallography and Photonics' RAS, Moscow) for supplying the samples.

Funding information

This study was supported by the Scholarship of the President of the Russian Federation (No. SP-1445.2016.1) and performed within the research theme 'Development and application of methods of the diagnostics of inorganic, organic and bioorganic materials using X-ray and synchrotron radia-

tion, electrons and neutrons'. The experiments were performed using the equipment of the Shared Research Center of the Institute of Crystallography, Russian Academy of Sciences.

References

Baranov, A. I. (2003). *Crystallogr. Rep.* **48**, 1012–1037.

Baranov, A. I., Khiznichenko, V. P. & Shuvalov, L. A. (1989). *Ferroelectrics*, **100**, 135–141.

Baranov, A. I., Shuvalov, L. A. & Shchagina, N. M. (1982). *JETP Lett.* **36**, 459–462.

Becker, P. J. & Coppens, P. (1974). *Acta Cryst.* A**30**, 129–147.

Chen, R. H., Chen, T. M. & Shern, C. S. (2000). *J. Phys. Chem. Solids*, **61**, 1399–1406.

Dmitricheva, E. V., Makarova, I. P. & Grebenev, V. V. (2015). *Crystallogr. Rep.* **60**, 814–820.

Dmitricheva, E. V., Makarova, I. P., Grebenev, V. V., Dolbinina, V. V. & Verin, I. A. (2014*a*). *Crystallogr. Rep.* **59**, 344–352.

Dmitricheva, E. V., Makarova, I. P., Grebenev, V. V., Dolbinina, V. V. & Verin, I. A. (2014*b*). *Solid State Ionics*, **268**, 68–75.

Dmitricheva, E. V., Makarova, I. P., Grebenev, V. V., Dolbinina, V. V., Verin, I. A., Chitra, R. & Choudhury, R. R. (2014). *Crystallogr. Rep.* **59**, 878–884.

Fitzergerald, R. (2001). *Phys. Today*, **54**, 22–24.

Fukami, T., Horiuchi, K., Nakasone, K. & Furukawa, K. (1996). *Jpn. J. Appl. Phys.* **35**, 2253–2254.

Haile, S. M., Chisholm, C. R. I., Sasaki, K., Boysen, D. A. & Uda, T. (2007). *Faraday Discuss.* **134**, 17–39.

Ivanov-Schitz, A. K. & Murin, I. V. (2010). *Solid State Ionics*, Vol. 2. St Petersburg: SPb University Press.

Lim, A. R. & Ichikawa, M. (2006). *J. Solid State Chem.* **179**, 117–121.

Lindner, L., Zdanowska-Frączek, M., Pawłowski, A. & Frączek, Z. J. (2014). *J. Appl. Phys.* **116**, 163513.

Łukaszewicz, K., Pietraszko, A. & Augustyniak, M. A. (1993). *Acta Cryst.* C**49**, 430–433.

MacDonald, J. R. (1987). *Impedance Spectroscopy: Emphasizing Solid Materials and Systems*. Wiley: New York.

Makarova, I. (2015). *Phys. Solid State*, **57**, 442–449.

Makarova, I. P., Chernaya, T. S., Filaretov, A. A., Vasil'ev, A. L., Verin, I. A., Grebenev, V. V. & Dolbinina, V. V. (2010). *Crystallogr. Rep.* **55**, 393–403.

Makarova, I., Grebenev, V., Dmitricheva, E., Dolbinina, V. & Chernyshov, D. (2014). *Acta Cryst.* B**70**, 218–226.

Matsuo, Y., Kawachi, S., Shimizu, Y. & Ikehata, S. (2002). *Acta Cryst.* C**58**, i92–i94.

Melzer, R. (1996). *Solid State Ionics*, **92**, 119–127.

Mkarova, I. P., Shuvalov, L. A. & Simonov, V. I. (1988). *Ferroelectrics*, **79**, 111–116.

Norby, T. (2001). *Nature*, **410**, 877–878.

Otomo, J. (2003). *Solid State Ionics*, **156**, 357–369.

Oxford Diffraction. (2011). *CrysAlis PRO* and *SCALE3 ABSPACK*. Oxford Diffraction Ltd, Yarnton, Oxfordshire, UK.

Pavlenko, N., Pietraszko, A., Pawlowski, A., Polomska, M., Stasyuk, I. V. & Hilczer, B. (2011). *Phys. Rev. B*, **84**, 064303.

Pawlowski, A., Pawlaczyk, Cz. & Hilczer, B. (1990). *Solid State Ionics*, **44**, 17–19.

Petriček, V., Dušek, M. & Palatinus, L. (2014). *Z. Kristallogr.* **229**, 345–352.

Ramasastry, C. & Ramaiah, K. S. (1981). *J. Mater. Sci.* **16**, 2011–2016.

Schwalowsky, L., Vinnichenko, V., Baranov, A., Bismayer, B., Merinov, B. & Eckold, G. (1998). *J. Phys. Condens. Matter*, **10**, 3019–3027.

Selezneva, E. V., Makarova, I. P., Grebenev, V. V. & Komornikov, V. A. (2018). *Crystallogr. Rep.* In the press.